Unsteady Aerodynamic Analysis around Oscillating Ahmed body by LS-DYNA ver.980

Hiroyuki Sawamoto Tsuyoshi Yasuki, Hiroshi Tanaka, Kazuyoshi Ishii
Toyota Motor Corporation

Abstract

This paper describes an aerodynamic effect of the Ahmed body model in sinusoidal pitching motion. Relationships of pitching angle to lift coefficient were analyzed by computational fluid dynamics (CFD) of LS-DYNA ver.980. Those numerical results showed good agreements with wind tunnel test results reported in the past. The flow field was investigated by using this numerical analysis result and the relationship of bottom surface pressure distribution to the lift coefficient was clarified.

1 Introduction

In recent years computational fluid dynamics (CFD) has been used in a variety of different engineering fields. In the automotive industry, it has been used to analyze how to reduce air resistance of cars. This analysis has involved a simulated wind tunnel testing assuming steady vehicle running under constant wind speed and wind direction conditions. However, under actual driving conditions, aerodynamic forces affect vehicle behaviour due to dynamic changes in the vehicle attitude and wind direction. These conditions are very difficult to measure, calculate, and analyze from a technological stand point because the relative positions of the vehicle body, road surface, and tires are always changing. Previous research included an experimental analysis using models that consider dynamic changes in vehicle attitude, such as pitching and heaving motions to simulate actual driving conditions [1]. There were not many examples of research using computational analysis of the relationship between the vehicle attitude and aerodynamic lift.
This paper describes an Ahmed model with pitching motion that was used to simulate the changes in vehicle attitude during driving to calculate the flow of air. This paper also reports the results that were obtained from analyzing the vehicle attitude and aerodynamic lift.

2 Numerical simulation method

2.1 Solver

CFD code of LS-DYNA ver.980 was used [2]. This CFD code solves Navier-Stokes equations (Equation (1)) and continuity equation (Equation (2)) with LES model (Equation (3)).

Navier-Stokes equation:

$$\rho\left(\frac{\partial u_i}{\partial t}+\left(u_j-v_j\right)\right)=-\frac{\partial p}{\partial x_i}+\mu\frac{\partial^2 u_i}{\partial x_j \partial x_j}+\rho f_i \qquad \ldots (1)$$

Continuity equation:

$$\frac{\partial u_i}{\partial x_i}=0 \qquad \ldots (2)$$

LES model:

$$\rho\left(\frac{\partial\tilde{U}_i}{\partial t}+\left(\tilde{U}_j-v_j\right)\frac{\partial\left(\tilde{U}_i\right)}{\partial x_j}\right)=-\frac{\partial\tilde{P}}{\partial x_i}+\frac{\partial}{\partial x_j}\left[\mu\frac{\partial\tilde{U}_i}{\partial x_j}+\mu_{sgs}\frac{\partial\tilde{U}_i}{\partial x_j}\right] \quad \ldots (3)$$

where, ρ is density, P is pressure, u is speed, and υ is mesh deforming velocity.

2.2 Computational model and grids

2.2.1 Computational model

The Ahmed model, proposed by Ahmed et al. [3], was used as the computational model. Figure 1 shows dimensions of the model. It had a total length of 1,044 mm and a height of 288 mm, while the slant angle on the back surface is 12.5 degrees. The central axis of rotation was placed on the bottom surface of the model at a point 522 mm from the back end.

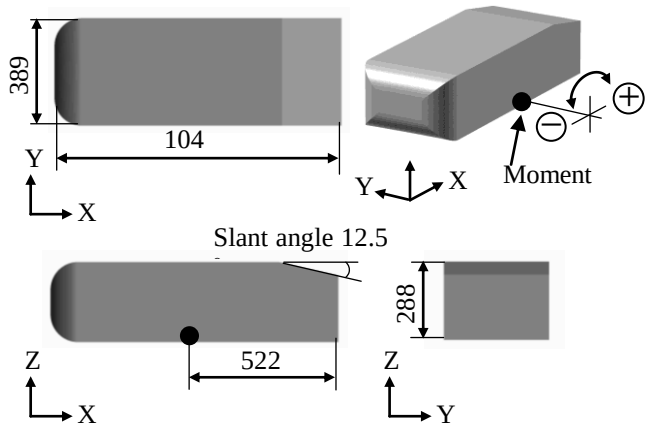

Fig. 1: model (units in mm)

2.2.2 Computational grids

Figure 2 shows the computational grid of the fluid used for the calculations. The number of grids was approximately 3,400,000 and a tetrahedral mesh was used. 5-layer prism mesh was also placed near the surface layer of the model, as shown in Figure 3.

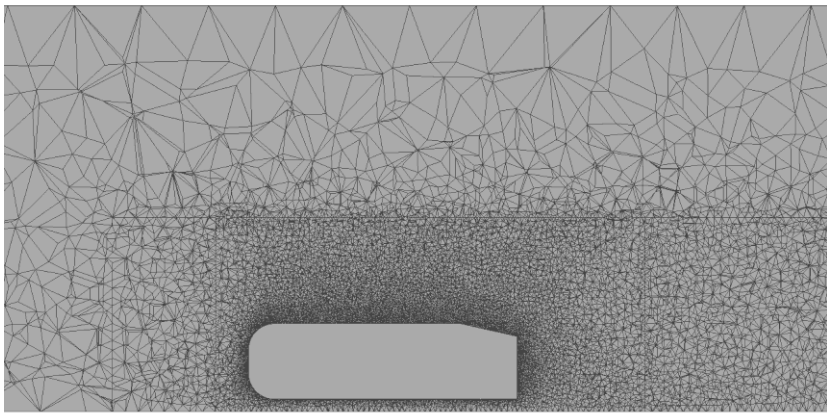

Fig. 2: Grids around Model

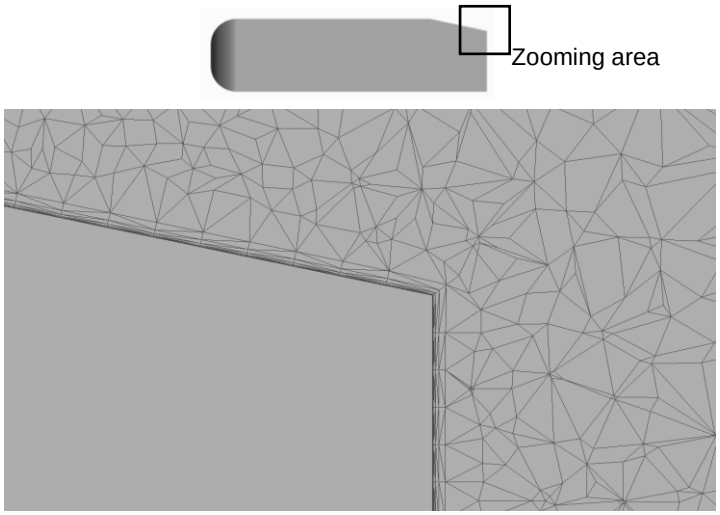

Fig. 3: Boundary layer mesh close to surface of the model

2.2.3 Boundary conditions

The analytical space used in this analysis has the same dimensions as the analytical space used by Inaki et al. [4]. In addition, an interior boundary was set to specify the mesh size that surrounds the model within the calculation domain (see Figure 4).
A constant flow rate of 40.0 m/s was applied to the inlet and a constant pressure of 101,325 Pa was applied to the outlet. The Reynolds number, which is the representative length of the total length of the model (L=1,044 mm), was Re=2,800,000. All of the walls of the calculation domain were set to free slip conditions (see Table 1).
Table 2 shows a list of the calculation case studies. Cases 1 to 3 were to examine the effect of the aerodynamic force (lift coefficient) at different vehicle attitudes with the model without oscillating motion on the aerodynamic force (lift coefficient) caused by differences in the frequency and amplitude when the model was forced to oscillate in a pitching motion.

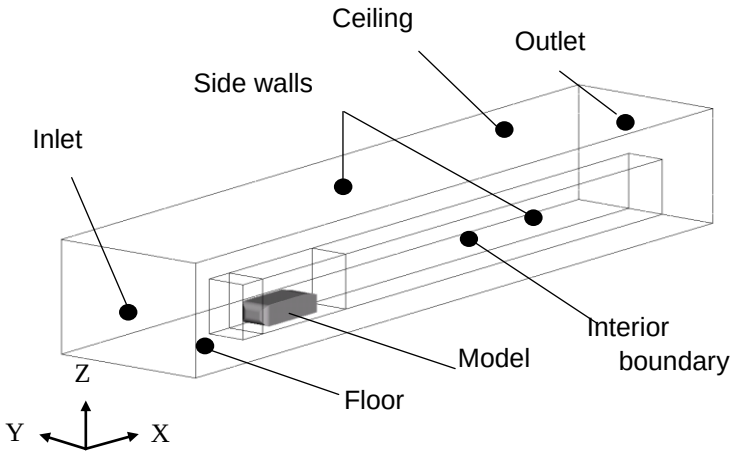

Fig. 4: Calculation domain

Table 1: Boundary conditions

Boundary	Condition
Inlet	40[m/s] Constant X Direction Velocity
Outlet	101325[Pa] Constant pressure
Sidewalls	Free slip
Floor	Free slip
Ceiling	Free slip

Table 2: Calculation cases

Case No.	Oscillation freq.	Amplitude
1	0Hz (Static)	0°
2	0Hz (Static)	+3°
3	0Hz (Static)	-3°
4	4Hz	±3°
5	8Hz	±3°
6	4Hz	±1.5°

3 Numerical simulation results

Figure 5 shows the simulation results in a static condition and at 0 degrees, where the Ahmed model was parallel to the surface of the floor (Here after referred as to “standard position”). The results of were compared with the results of the experiment referred from Kawakami et al. [5]. It was found that they showed fairly goof correlations. Figure 6 shows the calculation results obtained when the model was subjected to pitching motion. Once again, when these results were compared to the experimental results by Kawakami et al. [6], it was found that there was close correspondence between the pitching angle and the lift coefficient (CL).

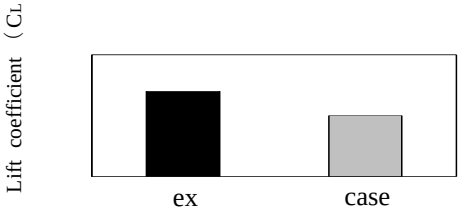

Fig. 5: Lift coefficient of static 0°Condition

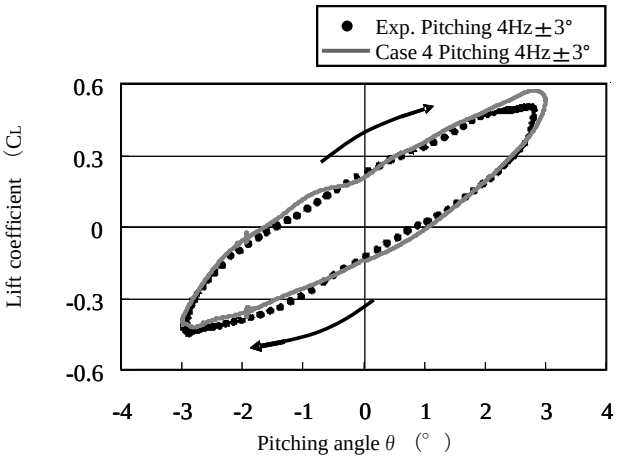

Fig. 6: Lift coefficient of pitching motion at 4Hz

Figure 7 shows the calculation results when the model was held in a static condition by changing pitch angle (cases 1 to 3). The lift coefficient increased when the pitch angle was increased i.e., the head of the model rose up.

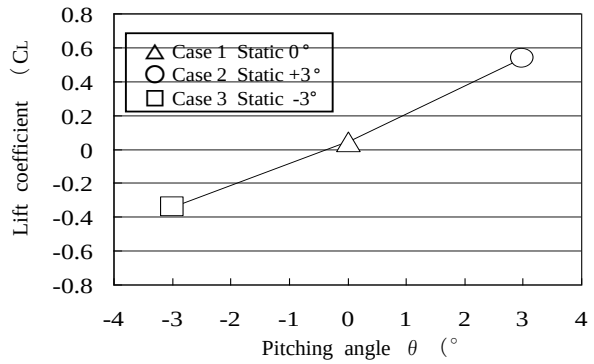

Fig. 7: Lift coefficient in static conditions

Figure 8 shows the calculation results when the frequency of the pitching motion was changed (cases 4 and 5). The fluctuation range of the lift coefficient in the standard position increased when the pitching frequency was increased.

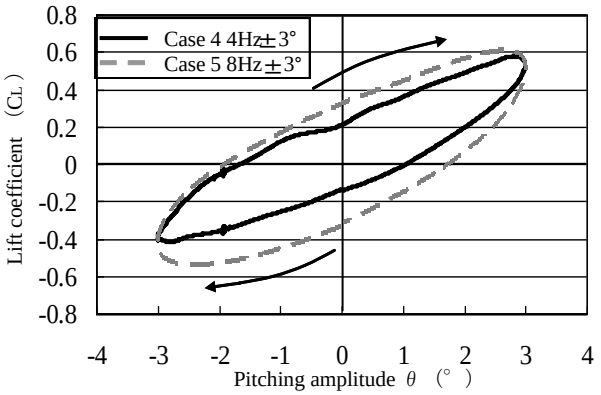

Fig. 8: Lift coefficient of pitching motion as a function of oscillating frequency

Figure 9 shows the calculation results when the amplitude of the pitching motion was changed (cases 4 and 6). The fluctuation range of the lift coefficient in the standard position decreased when the amplitude of the pitching motion was decreased.

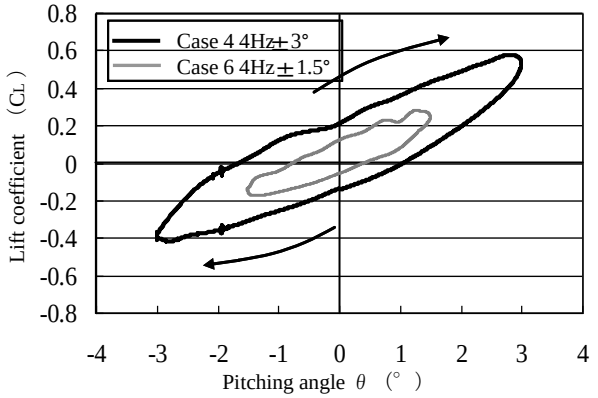

Fig. 9: Lift coefficient of pitching motion as a function as pitching angle

4 Discussion

The following three points are discussed in this research:
1) the lift coefficient of the model in a static condition,
2) the lift coefficient when the model is subjected to a pitching motion, and
3) the effects that the frequency and amplitude of the pitching motion have on the lift coefficient.

4.1 Lift Coefficient of Model in Static Condition

The cause of the increase in the lift coefficient when the pitch angle of the model was increased while in a static condition was examined. Figure 10 shows the pressure distributions on the top and bottom surfaces of the model when the model was held at different attitudes. It was found that there was a greater difference in the distribution of pressure on the bottom surface of the model than on the top surface, depending on the attitude. Since there was little change in the pressure distribution on the top surface of the model even when the attitude of the model was changed, it was decided to focus on the bottom surface. The pressure distributions on the bottom surface of the model (especially near the back) were compared and it was found that the pressure increased in order from case 3 to case 1 to case 2. This was consistent with the trend seen in the lift coefficient at the different attitudes. Therefore, it was surmised that the lift coefficient grows larger when the pressure on the bottom surface of the model increases.

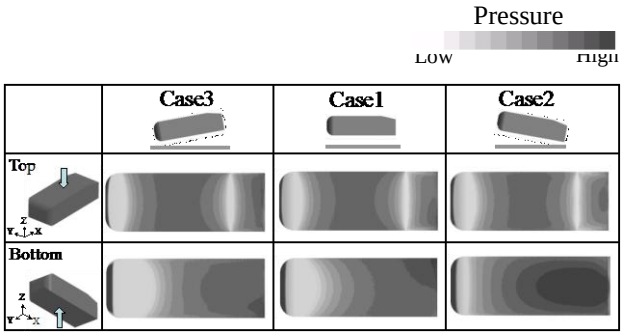

Fig. 10: Pressure distribution at static conditions

4.2 Lift Coefficient of Model during pitching motion

Figure 11 shows the difference in the lift coefficient between the static condition (cases 1 to 3) and when the pitching motion was applied (case 5). When the model is at its maximum amplitude (3 degrees), there is no difference in the lift coefficient of the model in the static condition and when the pitching motion is being applied. However, when the pitching motion is being applied and the head of the model is going up, the lift coefficient of the model in the standard position is higher than the lift coefficient of the model in the standard position in the static condition. It was also found that, when the pitching motion is being applied and the head of the model is going down, the lift coefficient of the model in the standard position is lower than the lift coefficient of the model in the standard position in the static condition. The following sections provide a more detailed comparison of the model when the pitching motion is being applied and in the static condition.

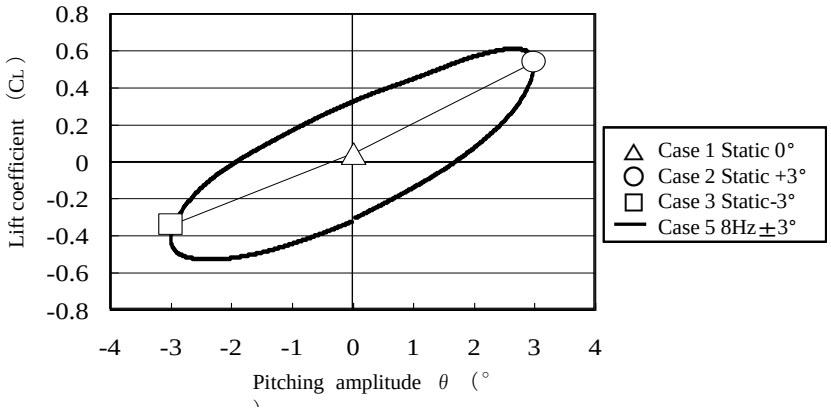

Fig. 11: Lift coefficient at static condition as a function of pitching angle

Figure 12 compare the pressure distribution on the bottom surface of the model when the pitching motion has reached its maximum amplitude (3 degrees) with the pressure distribution in the static condition. When the pitching motion of the model reaches its maximum amplitude i.e., the motion velocity is 0 m/s, the pressure distribution on the bottom surface of the model is equal to that in the static condition.

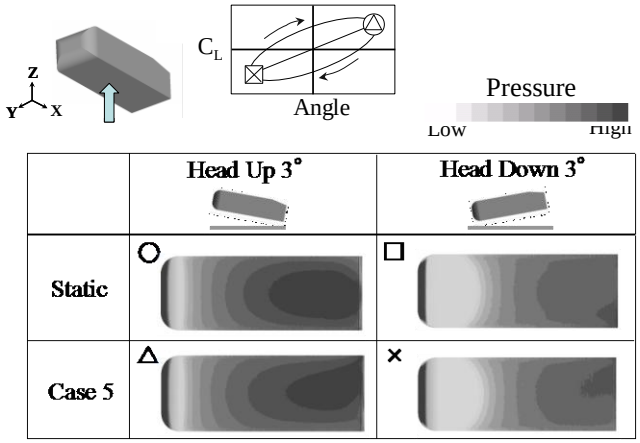

Fig. 12: Pressure distribution at bottom surface at the maximum displacement

Figure 13 compares the pressure distribution on the bottom surface of the model when the pitching motion has reached the standard position with the pressure distribution in the static condition. The pressure on the bottom surface when the pitching motion is being applied and the head of the model is going up, is higher than the pressure when the model is in the static condition. It was also found that the pressure on the bottom surface when the pitching motion is being applied and the head of the model is going down, is lower than the pressure when the model is in the static condition. Therefore, it was surmised that when the motion velocity of the pitching motion is at its maximum (i.e., when the model is in the standard position), the increase and decrease in the lift coefficient at this position causes the difference in pressure on the bottom surface of the model at its back end.

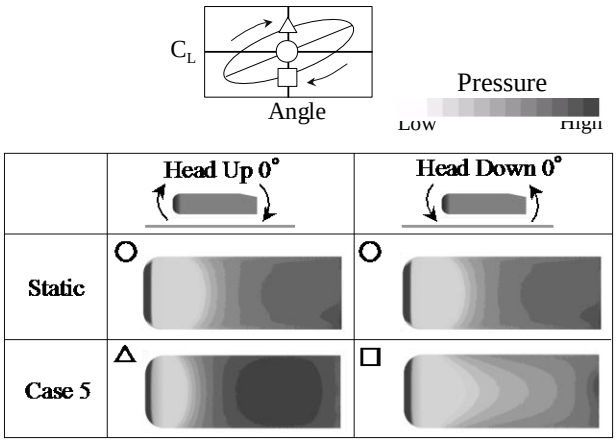

Fig. 13: Pressure distribution at bottom surface at initial position

Figure 14 shows the under body pressure distributions for each phase of the pitching motion at a cross section of the back of the model (Center of the slant) that is based on the calculation results from case 5. The under body pressure on the back cross section of the model increases as the head of the model goes up. When the model reaches the standard position as its head is going up, the pressure is high. In contrast, when the model reaches the standard position as its head is going down, the pressure is low. Therefore, the outflow and inflow of under body air corresponds to the movements of the model.

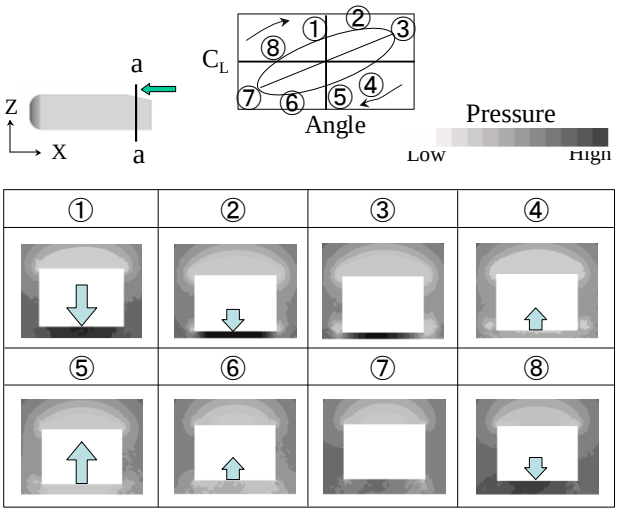

Fig. 14: Pressure distribution at a-a section

Figure 15 shows the directions of vertical vortices that are parallel to the direction of the main air flow and are formed on the side surfaces and bottom surface of the model for each phase of the pitching motion. These are also based on the calculation results from case 5. Therefore, the direction of rotation of the vertical vortices changes in a way that delays the phase in relation to the movement of the model.

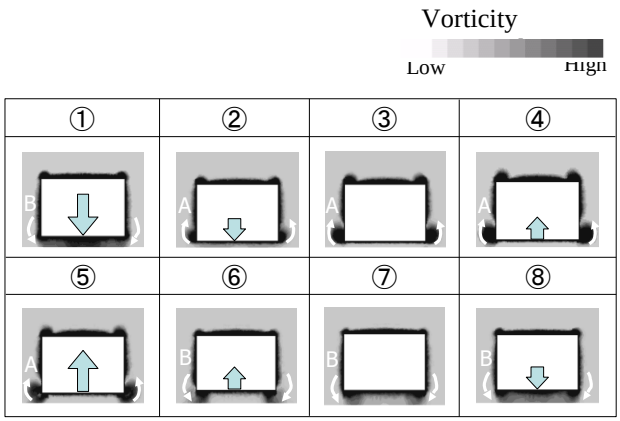

Fig. 15: Vorticity magnitude distribution at a-a section

Figure 16 shows the relationship between the under body pressure and the vertical vortices when the model is at the standard position when its head is going up and when its head is going down. It is surmised that the increase and decrease in the lift coefficient at the standard position when the pitching motion is being applied to the model is due to the inflow and outflow of under body air caused by the movement of the model. Another cause is the vertical vortices, which are moving in a direction that intensifies the change in pressure.

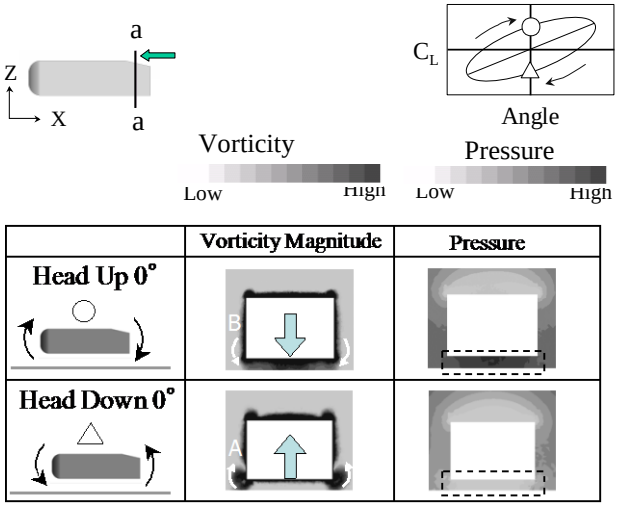

Fig. 16: Comparison vorticity with pressure at a-a section

4.3 Effect of Frequency and Amplitude

Figures 8 and 9 show that the fluctuation range of the lift coefficient at the standard position is a function of frequency and amplitude of the pitching motion. The causes of this change in the fluctuation range were examined.

Figure 17 shows the under body pressure distributions at a cross section of the back of the model (Center of the slant) when the model is at the standard position both when the head is going up and when the head is going down. Figure 17 also shows the motion velocity of the back end of the model in the vertical direction when the pitching motion was applied. The calculation results from cases 4 to 6 were used for all the information in this figure. The higher that the pitching frequency becomes, the greater the difference in the under body pressure when the model is at the standard position, both when the head is going up and when the head is going down (a and b in Figure 17). The motion velocity is also fast. In contrast, the smaller that the pitching amplitude becomes, the lower the difference in the under body pressure when the model is at the standard position, both when the head is going up and when the head is going down (a and c in Figure 17). The motion velocity is also slow.

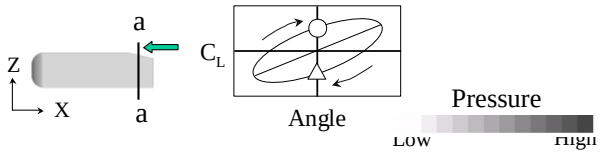

Case No.	Case 5	Case 4	Case 6
Oscillation Freq.	8Hz	4Hz	4Hz
Amplitude	3°	3°	1.5°
Pitch Motion Velocity	1.40m/s	0.70m/s	0.35m/s
Head Up 0°	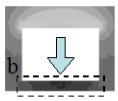	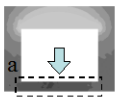	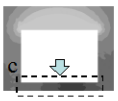
Head Down 0°	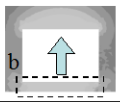	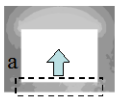	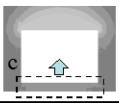

Fig. 17 Pressure distribution at a-a section as a function of pitching angles and frequencies

Figure 18 shows the directions of the vertical vortices that are parallel to the direction of the main air flow and are formed on the side surfaces and bottom surface of the model. It also shows the size of these vortices when the model is at the standard position both when the head is going up and when the head is going down. It was found that the higher the pitching frequency becomes, the larger that the vertical vortices become (a and b in Figure 18), while the smaller that the pitching amplitude becomes, the smaller that the vertical vortices become (a and c in Figure 18).
The following points were surmised from these results. When the pitching frequency is high, the difference in the under body pressure at the standard position both when the head is going up and when the head is going down becomes large, and the vertical vortices that intensify the change in pressure also become larger. These effects in turn cause the fluctuation range of the lift coefficient at the standard position to increase. In the same way, when the pitching amplitude is small, the difference in the under body pressure at the standard position both when the head is going up and when the head is going down is small, and the vertical vortices that intensify the change in pressure also become smaller. Consequently, these effects then cause the fluctuation range of the lift coefficient at the standard position to become smaller.

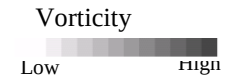

Case No.	Case 5	Case 4	Case 6
Oscillation Freq.	8Hz	4Hz	4Hz
Amplitude	3°	3°	1.5°
Head Up 0°	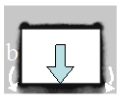		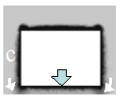
Head Down 0°	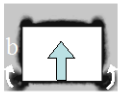		

Fig. 18: Vorticity magnitude distribution at a-a section as a function of pitching angles and frequencies

Next, Fig. 19 shows a summary of the relationship between the motion velocity of the back end of the model in the vertical direction when the pitching motion was applied in cases 4 to 6 (as shown in Fig. 17) and the under body pressure at a representative point at the back of the model (Center of the slant). The motion velocity and the under body pressure correlate well in an almost proportional relationship.

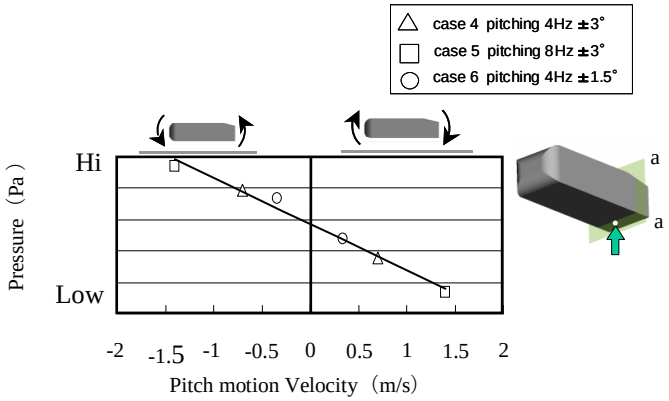

Fig. 19: Relationships between pitching velocity and pressure of bottom surface at a-a section

5 Conclusion

The flow of air around an Ahmed model to which a pitching motion was forcibly applied was calculated to examine the relationship between the movement of the body and the aerodynamic force i.e., the lift coefficient.
The relationship between the pitching motion and the lift coefficient was found to be a curve in the clockwise direction and the results corresponded closely to the experimental results.
The lift coefficient when a pitching motion is applied to the model is generated by the change in pressure on the bottom surface of the model at its back end. This lift coefficient was found to have a close correlation with the motion velocity of the model.

References

[1] Kojima, Y., Ohta, H., Murata, O., Effects of aerodynamics on the longitudinal motion of a high-speed vehicle: 1st Report, Formulations of the aerodynamic characteristics, Journal of JSME, C, Vol. 60, No. 579（1994-11）, pp.3822-3828, (1994)

[2] Livermore Software Technology Corporation : LS-DYNA ver.980, User's Manual

[3] Ahmed, S. R., Ramm, G. and Faltin, G., Some salient features of the time-averaged ground vehicle wake, SAE Paper, No.840300, (1984).

[4] Inaki, C., Facundo, D. P. and Vincent, L., Incompressible CFD results using LS-DYNA for high Raynolds number flow around bluff bodies, 8th European LS-DYNA Users Conference, Strasbourg, (2011).

[5] Kawakami, M., Sato., N., Aschwanden, P., Kato, Y., Nakagawa, M., Ono, E., A modeling of unsteady aerodynamic forces based on the aerodynamic analyses around a simplified car model in periodic motions (Mechanical systems), Journal of JSME, C, Vol.76, No.768 (2010-8) , pp2006-2015, (2010).